THE DESIGN AND EVALUATION OF A VOIGT EFFECT COHERENT FORWARD SCATTERING ATOMIC SPECTROMETER

BY

LORI ANN DAVIS

A DISSERTATION PRESENTED TO THE GRADUATE SCHOOL
OF THE UNIVERSITY OF FLORIDA IN
PARTIAL FULFILLMENT OF THE REQUIREMENTS
FOR THE DEGREE OF DOCTOR OF PHILOSOPHY

UNIVERSITY OF FLORIDA

1986

To my parents,
without whose support,
none of this
would have been possible.

ACKNOWLEDGMENTS

I am grateful to Chester Eastman, Dailey Burch, Vernon Cook and Arthur Grant of the Chemistry Department for the construction of much of the instrumentation used in this work.

I also wish to thank Dr. Benjamin Smith and Dr. Edward Voigtman for their invaluable help and suggestions during my graduate career. Dr. Nicolo Omenetto was also of great help with his inspiring enthusiasm. Special thanks are extended to Dr. Robert J. Krupa for his assistance, support, and encouragement which made my stay at the University of Florida an enjoyable experience.

A special debt of gratitude is extended to Dr. James D. Winefordner for his encouragement and understanding. His enthusiasm for research and life serves as an inspiration to those around him. It has been a privilege and a valuable learning experience to be a part of his research group for the past 4 years.

TABLE OF CONTENTS

Page

ACKNOWLEDGMENTS....................iii

LIST OF TABLES....................v

LIST OF FIGURES....................vi

ABSTRACT....................viii

CHAPTERS

1 INTRODUCTION....................1

2 ZEEMAN ATOMIC ABSORPTION SPECTROMETRY....................3

3 THEORY OF COHERENT FORWARD SCATTERING ATOMIC SPECTROMETRY....................16

4 EXPERIMENTAL....................31

5 NOISE CHARACTERISTICS OF A VOIGT EFFECT CFS SPECTROMETER....................39

6 LASER-EXCITED CFS....................54

7 MULTI-ELEMENT CFS....................60

8 THE FUTURE OF CFS IN ANALYTICAL CHEMISTRY....................67

9 CONCLUSIONS....................70

APPENDICES

I THE DERIVATION OF A GENERAL EQUATION FOR A VOIGT EFFECT CFS SPECTROMETER....................71

II LIST OF ABBREVIATIONS....................76

REFERENCES....................77

BIOGRAPHICAL SKETCH....................82

LIST OF TABLES

Table | Page

1 SPLITTING PARAMETERS AND TRANSITION PROBABILITIES OF MANY ELEMENTS....................9

2 LIMITS OF DETECTION IN mg/L (S/N = 3) FOR Ca AT 422.673 nm USING AMPLITUDE MODULATION (AM) VS. DC MEASUREMENT....................52

3 LIMITS OF DETECTION (S/N = 3) FOR LASER-EXCITED CFS........58

4 LIMITS OF DETECTION (S/N = 3) FOR MULTI-ELEMENT CFS........65

LIST OF FIGURES

Figure Page

1 Energy Level Diagram for a Normal Zeeman Splitting Pattern ($^1S_0$ - $^1P_1$ transition)....................4

2 Voigt Profile of the Absorbance Line for Sr at 460.7332 nm in a 1.2 Tesla Magnetic Field Exhibiting a Normal Zeeman Splitting Pattern ($^1S_0$ - $^1P_1$ transition)....................5

3 Energy Level Diagram for an Anomalous Zeeman Splitting Pattern ($^2S_{1/2}$ - $^2P_{3/2}$ transition)....................7

4 Examples of Several Zeeman Splitting Patterns Seen in a Transverse Magnetic Field....................10

5 The Anomalous Dispersion Function for Sr at 460.7332 nm in a 1.2 Tesla Magnetic Field Exhibiting a Normal Zeeman Splitting Pattern ($^1S_0$ - $^1P_1$ transition)....................17

6 Model for the Incident Light in a Voigt Effect CFS Spectrometer....................20

7 Model for the Dichroic Contribution to the CFS Signal in a Voigt Effect Spectrometer....................21

8 Profile of the Dichroism of Sr at 460.7332 nm in a 1.2 Tesla Magnetic Field for a Voigt Effect CFS Spectrometer....................23

9 Model for the Birefringent Contribution to the CFS Signal in a Voigt Effect Spectrometer....................24

10 Profile of the Birefringence of Sr at 460.7332 nm in a 1.2 Tesla Magnetic Field for a Voigt Effect CFS Spectrometer....................26

11 Block Diagram for the Multi-Element CFS Spectrometer......32

12 Block Diagram for the Laser-Excited CFS Spectrometer......35

13 Background Spectrum for the Fuel Rich Air-Acetylene Flame..40

14 Background Spectra for the Xenon Arc Lamp Through Crossed Polarizers Using a Lock-in Amplifier With (a) and Without (b) the Flame On..........................42

15 The Background Spectrum for the Squared CFS System ($\theta = 90^\circ$)...43

16 The Background Spectrum for the Linear CFS System ($\theta = 98.5^\circ$)...45

17 The Noise Power Spectrum for the Squared CFS System Taken at 306 nm...47

18 The Noise Power Spectra for the Linear CFS System Taken at 306 nm...48

19 CFS and AES Curves of Growth for Ca at 422.673 nm With the Squared CFS System Using DC Measurement..........50

20 CFS Curve of Growth for Na at 589.0 nm in a Flame Using Laser Excitation.....................................55

21 Plot of the Laser Intensity vs. the CFS Signal in a Flame..57

22 CFS Curve of Growth for Na at 589.0 nm in a Flame Using Continuum Excitation................................61

23 CFS Curve of Growth for Ca at 422.673 nm in a Flame Using Continuum Excitation................................62

24 CFS Curve of Growth for Cu at 324.754 nm in a Graphite Furnace Using Continuum Excitation...............64

Abstract of Dissertation Presented to the Graduate School
of the University of Florida in Partial Fulfillment of the
Requirements for the Degree of Doctor of Philosophy

THE DESIGN AND EVALUATION OF A VOIGT EFFECT COHERENT FORWARD SCATTERING ATOMIC SPECTROMETER

BY

LORI ANN DAVIS

August, 1986

Chairman: James D. Winefordner
Major Department: Chemistry

Coherent forward scattering atomic spectrometry consists of the magneto-optic rotation of light by atoms at their resonance transitions. A system was constructed using a transverse magnetic field, the Voigt effect, surrounding an atom reservoir. Both an air-acetylene flame and a graphite furnace are used in this system. The incident light is polarized by a calcite prism polarizer at a 45° angle to the magnetic field. A second polarizer, the analyzer, is placed at a 90° angle to the first polarizer, to detect the light which is rotated by the atoms. With the polarizers oriented orthogonal to each other, the signal produced is proportional to the square of the atom concentration. The signal can be linearized with respect to atom concentration by offsetting the analyzer by a small offset angle. The linearization causes a change in the noise characteristics of the CFS system. A comparison of amplitude modulation vs DC measurement also showed different results when squared results were compared to linear results. A continuum source was used to evaluate the multi-element capabilities of CFS in terms of limits of detection (LODs), linear dynamic ranges, and other figures of merit. In an attempt to improve the figures of merit of the system, a nitrogen laser, which was unsuccessful for a variety of reasons, was also used. It is, however, the multi-element capabilities of CFS which provide future interest in the field of analytical chemistry.

CHAPTER I
INTRODUCTION

In 1862, Zeeman established beyond any doubt that the periodic time of vibration of a source of monochromatic light is altered when the source is placed in a magnetic field (1). It was not until 1955 that Walsh developed the first atomic absorption spectrophotometer (AAS) (2). Prugger, in 1968, applied the Zeeman effect to background correction in AAS (ZAAS) (3,4). Hollander et al. in 1970 (5) and Parker in 1971 (6) made further advances in the use of the Zeeman effect in AAS. In 1971, Scintex, Ltd. of Canada released the first commercial instrument for ZAAS which monitored Hg in ambient air. An instrument which was applicable to all elements was developed by Hitachi, Ltd. in 1976 (7) using Inverse ZAAS while Grün Optik developed an instrument using Direct ZAAS in 1979. Since that time, many reviews have appeared in the literature on ZAAS (8,9).

The magneto-optic rotation of polarized light by atoms in a magnetic field was first observed by Hanle in 1924 (10). The fundamental theory of forward scattering of resonance radiation was first derived by Corney, Kibble, and Series (11). Further theoretical evaluations of coherent forward scattering (CFS) atomic spectrometers have been done for both the Voigt effect and the Faraday effect, a transverse and a longitudinal magnetic field, respectively (12-20). Church and Hadeishi first suggested the use of CFS as an analytical technique (21). Since that time, a variety of CFS systems have been evaluated using line sources (21-25) and continuum sources (26-29) as excitation sources. An increasing interest has occurred in CFS as a multi-element analytical technique, to the extent that Koirtyohann has touted CFS as a new technique of the 80s (30).

CHAPTER 2
ZEEMAN ATOMIC ABSORPTION SPECTROMETRY

The use of the Zeeman effect for background correction has been demonstrated to be analytically useful in AAS (7,31-47). When atoms are located in a magnetic field, the atomic energy levels of those atoms are split causing the atomic transitions to also be split. This splitting is due to the fact that the magnetic quantum numbers are no longer degenerate in terms of energy in a magnetic field and can range from +J to -J with $\Delta M = 0, \pm 1$, for atomic transitions. In a normal Zeeman splitting pattern, $^1S_0-^1P_1$, the atomic transition splits into 3 components, 1 π component ($\Delta M = 0$) and 2 σ components ($\Delta M = \pm 1$) (see Figure 1). The energy diagram shows the splitting of the excited state causing the atomic emission and atomic absorption to be split into 3 components. Figure 2 shows a Voigt profile atomic absorption spectrum (calculated using numerical integration) in a 1.2 T magnetic field for Sr at 460.7332 nm, which has a normal Zeeman splitting pattern. The π component remains at the resonance frequency of the transition and absorbs polarized light whose electric vector is parallel to the magnetic field. The 2 σ components split to either side of the resonance line and absorb polarized light whose electric vector is perpendicular to the magnetic field. This normal Zeeman splitting pattern is the simplest type of splitting pattern seen in the spectral lines of Be, Mg, Ca, Ba, Zn, Cd, and Hg as well as Sr.

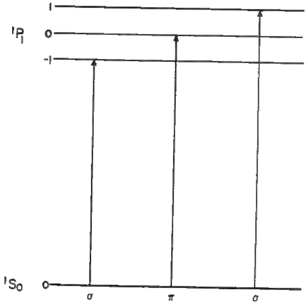

Figure 1 Energy Level Diagram for a Normal Zeeman Splitting Pattern ($^1S_0$ - $^1P_1$ transition)

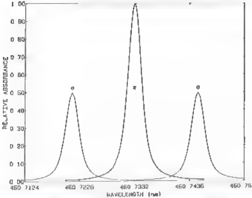

Figure [illegible]. Voigt Profile of the Absorbance Line for Sr at 460.7332 nm in a [illegible] T Magnetic Field Exhibiting a Normal Zeeman Splitting Pattern ($^1S_0$ – $^1P_1$ transition)

Many elements, however, do not have this simple splitting pattern and exhibit anomalous Zeeman splitting patterns. Anomalous Zeeman splitting patterns occur when the ground state and the excited state exhibit splitting. The splitting pattern of a $^2S_{1/2}$-$^2P_{3/2}$ transition as seen in Cu, K, Na, Rb, Li, Cs, and Au is seen in Figure 3. Both the ground state and the excited state split; however, the splitting energy in the ground state is not equal to that in the excited state. Because of this difference in the splitting, the 3 components, seen in a normal Zeeman pattern, are again split resulting in a total of 6 components; see Figure 3. As can be seen in Table 1, which lists the strong transitions of many elements, most elements do not exhibit a normal Zeeman splitting pattern. A variety of splitting patterns, given by Yasuda et al. (8), is shown in Figure 4. The normal Zeeman splitting pattern is shown in Category I. It should be noted that the transitions $^3P_2$-$^3P_2$ and $^3P_2$-$^3P_1$ also show this type of splitting pattern, despite the fact splitting occurs in both the ground state and the excited state energy levels of these transitions. Since both the ground state and the excited state are designated as ^3P, they will exhibit the same splitting in energy in both states, thus making any further splitting of the π and σ components degenerate. The transitions listed in Table 1 are also grouped according to their splitting. The transitions $^2P_{3/2}$-$^2D_{5/2}$, $^4S_{3/2}$-$^4P_{5/2}$, and $^4S_{3/2}$-$^3D_{5/2}$ show splitting patterns similar to Category V, but much less complicated with all 3 components each splitting into 4 components. The transitions, $^6S_{5/2}$-$^6P_{5/2}$, $^7S_3$-$^7P_3$,

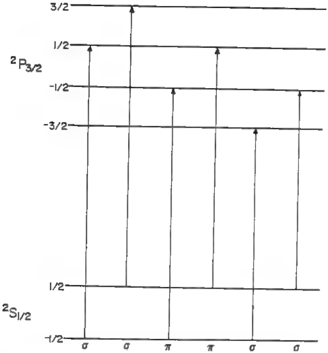

Figure 3 Energy Level Diagram for an Anomalous Zeeman Splitting Pattern ($^2S_{1/2}$ - $^2P_{3/2}$ transition)

Table . SPLITTING PARAMETERS AND TRANSITION PROBABILITIES OF MANY ELEMENTS

DESIGNATION	ELEMENT	WAVELENGTH(nm)	gf(48)
$^{1}S_{0} - {}^{1}P_{1}$	Be	553.548	0.90
	Cd	228.802	0.92
	Ca	422 673	0.28
	Mg	285.213	1.1
	Hg	253.652	0.34
	Sr	460.733	0.27
	Zn	213.856	1.3
$^{3}P_{0} - {}^{3}P_{1}$	Pb	283.306	0.22
	Si	251.432	0.54
	Sn	286.333	0.65
$^{3}P_{1}\ \ {}^{3}P_{0}$	Si	252.411**	0.80
$^{5}D_{0} - {}^{5}D_{1}$	W	255 .35	0.80
$^{3}P_{2}\ \ {}^{3}P_{2}$	Si	251.611**	1.3
$^{3}P_{2}\ \ {}^{3}P_{1}$	Pb	405.783**	2.3
$^{2}S_{1/2}\ \ {}^{2}P_{1/2}$	Ag	328.068	0.53
	Na	589.592	0.47
$^{2}P_{1/2} - {}^{2}S_{1/2}$	Tl	377.572	0.22
$^{2}S_{1/2} - {}^{2}P_{3/2}$	Cs	455.536	0.42
	Cu	324.754	0.64
	Au	242 795	0.16
	Li	670.784	0 80
	K	766.491	1.4
	Rb	780.023	2.7
	Na	588 995	0.95

Table 1 --continued.

DESIGNATION	ELEMENT	WAVELENGTH(nm)	gf(48)
${}^2P_{1/2} - {}^2D_{3/2}$	Al	308.216	0.38
	Ga	287.424	0.73
	In	303.936	0.99
	Tl	276.787	0.47
${}^2P_{3/2} - {}^2S_{1/2}$	Tl	535.046**	0.92
${}^2P_{3/2} - {}^2D_{5/2}$	Al	309.271**	0.79
	Ga	294.364**	1.5
${}^4S_{3/2} - {}^4P_{5/2}$	Bi	206.170	0.38
${}^4S_{3/2} - {}^4D_{5/2}$	Bi	195.389	0.16
${}^6S_{5/2} - {}^6P_{5/2}$	Mn	279.827	0.78
${}^7S_3 - {}^7P_3$	Mo	317.035	0.82
${}^7S_3 - {}^7D_3$	Mo	315.816	0.57
${}^7S_3 - {}^7P_4$	Mo	313.259	1.4
	Cr	357.869	1.4
${}^3D_3 - {}^1G_4$	Pt	265.945	0.87
${}^5D_4 - {}^5F_5$	Fe	248.327	3.1
${}^3F_4 - {}^3G_5$	Ni	232.003	0.86
${}^5F_5 - {}^4G_4$	Ru	273.572	1.2
${}^4F_{9/2} \quad {}^4G_{11/2}$	Co	240.725	2.2
	Rh	343.489	0.73

** not a ground state transition

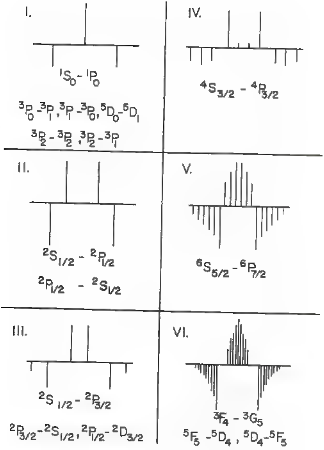

Figure 4. Examples of Several Zeeman Splitting Patterns Seen in a Transverse Magnetic Field

and $^7S_3$-$^7D_3$, show splitting patterns similar to Category IV with more splitting. The $^6S_{5/2}$-$^6P_{5/2}$ transition will have 16 total components, with the π component splitting into 6 components and the 2 σ components splitting into 5 components. The $^7S_3$-$^7P_3$ and $^7S_3$-$^7D_3$ will have the same type of splitting with a total of 19 components. The $^7S_3$-$^7P_4$ and $^3D_3$-$^1G_4$ transitions will have a splitting pattern similar to Category VI with a total of 27 components. The most complicated splitting pattern in Table 1 is the $^4F_{9/2}$-$^4G_{11/2}$ transition which will resemble the splitting pattern shown in Category V with a total of 30 components. Thus it can be seen that the splitting patterns for most atomic transitions are more complicated than the normal Zeeman splitting patterns discussed in most studies.

Several authors have reviewed the theory of Zeeman AAS in recent years (8,9). Yasuda et al. described the Zeeman effect (8) as follows. The Voigt function of the absorption coefficient (κ, ν at frequency ν), which is a convolution of the Doppler broadening, a Gaussian function, and the pressure broading, a Lorentzian function, is given in Equation [1].

$$k(\nu) = \kappa_0 \frac{a}{\pi} \int_{-\infty}^{\infty} \frac{e^{-y^2} dy}{a^2+(\omega - y)^2} \qquad [1]$$

$$a = \frac{\Delta\nu_L}{\Delta\nu_D} (\ln 2)^{1/2} \qquad [2]$$

$$\Delta\nu_L = 1.95\times10^{19} p\sigma L^2 \left[\frac{2R}{\pi T}\left(\frac{1}{M} + \frac{1}{M_p}\right)\right]^{1/2} = \text{half width of pressure broadened line (Hz)} \qquad [3]$$

$$\Delta\nu_S = \gamma\Delta\nu_L = \text{half width of pressure shift (Hz)} \qquad [4]$$

$$\Delta\nu_D = \frac{2(2R\ln 2)^{1/2}}{c}\,\nu_0\left(\frac{T}{M}\right)^{1/2} = \text{Doppler half width (Hz)} \qquad [5]$$

$$y = \frac{2(\nu-\nu_0)}{\Delta\nu_D}(\ln 2)^{1/2} \qquad [6]$$

$$K_0 = \frac{2}{\Delta\nu_D}\left(\frac{\ln 2}{\pi}\right)^{1/2} \cdot \frac{\pi e^2}{mc} \cdot Nf \ (m^{-1}) \qquad [7]$$

In the above equations, ν_0 is the frequency at the center of the line (Hz), c is the velocity of light in a vacuum (m/s), R is the gas constant, T is the absolute temperature (K), M is the atomic weight of the atom, m and e are the mass and charge of an electron, N is the number density of atoms in the ground state, f is the oscillator strength, p is the partial pressure of the perturbers, σ_L^2 is the effective cross section for collision between an atom and a perturber, Mp is the atomic or molecular weight of the perturber, and γ is the ratio of the shift to pressure broadening. In a magnetic field the atomic absorption line splits into its Zeeman components. The shift in the atomic energy level (ΔT_M in cm^{-1}) is given in the following equation:

$$-\Delta T_M = -M \cdot g \cdot L \cdot B \qquad [8]$$

where B is magnetic induction in G, M is the magnetic quantum number, L is the Lorentz unit, and g, the Landé factor, is defined in the following equations.

$$L = \frac{e}{4\pi mc^2} \; (= 4.67\text{x}10^{-5}\,\text{cm}^{-1}\text{G}^{-1}) \qquad [9]$$

$$g = 1 + \frac{J(J+1)+S(S+1)-L(L+1)}{2J(J+1)} \qquad [10]$$

where S is the total spin quantum number, L is the total orbital angular momentum quantum number, and J is the total angular momenta quantum number. The transition intensities (I) of the Zeeman components may be calculated with the following equations:

$$\Delta J=0 \quad \begin{cases} \Delta M=0 & I=4AM^2 \qquad [11] \\ \Delta M=\pm 1 & I=A(J\pm M+1)(J\mp M) \qquad [12] \end{cases}$$

$$\Delta J=\pm 1 \quad \begin{cases} \Delta M=0 & I=4B(J+M+1)(J-M+1) \qquad [13] \\ \Delta M=\pm 1 & I=B(J\pm M+1)(J\pm M+2) \qquad [14] \end{cases}$$

where A and B are constants. If the Zeeman components are summed together, the absorption line profile in a magnetic field ($k^a(\nu)$) can be described by the following equation:

$$k^a(\nu) = \sum_i k_{0i} \frac{a}{\pi} \int_{-\infty}^{+\infty} \frac{e^{-y_i^2} d y_i}{a+(\omega_i'-y_i)^2} \; \text{m}^{-1} \qquad [15]$$

$$\omega_i' = \frac{2(\nu-\nu_0+\Delta\nu_S+\Delta\nu_Z)}{\Delta\nu_D} (\ln 2)^{1/2} \qquad [16]$$

$$y_i = \frac{2(\nu-\nu_0+\Delta\nu_Z)}{\Delta\nu_D} (\ln 2)^{1/2} \qquad [17]$$

where $\Delta\nu_z$ is the Zeeman shift in Hz. De Loos-Vollebregt and De Galan have reviewed the theory of Zeeman AAS and discuss the limiting cases for those ZAAS systems commercially available (9).

The experimental set-up of a ZAAS system resembles that of a conventional AAS system with the addition of a magnet and a polarizer. The ZAAS systems are separated into two categories depending on the location of the magnet, Direct ZAAS and Inverse ZAAS. Direct ZAAS systems position the magnetic field around the hollow cathode lamp or EDL so that the emission from the lamp is split into its Zeeman components. The major difficulty in this approach is the design of a source which can be ignited in a magnetic field (8). An Inverse ZAAS system employs the magnetic field around the atom reservoir, which presents its own difficulties in the design of an atom reservoir which can be placed inside the poles of an electromagnet. An AC or a DC magnetic field may be employed with either system. The orientation of the polarizer is dependent on whether the magnet is AC or DC.

Both the Perkin Elmer and the Hitachi systems are Inverse Zeeman AAS systems (8) with the Hitachi system (7) employing a DC magnet and the Perkin Elmer system (49) employing an AC magnet. The background correction of both systems is based on the splitting of the σ components in a sufficient magnetic field outside of the profile of the hollow cathode lamp leaving only the background absorption. The Hitachi system uses a rotating polarizer to alternate measuring the σ components, the background absorption, and the π component, the atomic and background absorption. This modulation can be used to subtract the background absorption of the σ components from that of the π component, leaving only the atomic absorption of the π component. The Hitachi system, however, can exhibit a reduction in sensitivity for those elements which have anomalous Zeeman splitting patterns. If the π component of the atomic line splits outside of the profile of the hollow cathode, the sensitivity of the atomic absorption can be drastically reduced.

The Perkin Elmer system overcomes the sensitivity problem of the Hitachi system by using an AC magnetic field. In this system, the polarizer is oriented perpendicular to the magnetic field, so that the σ component is always observed (49). When the magnet is off, no splitting occurs, and atomic and background absorption are measured. When the magnet is on, the σ components are split outside of the profile of the hollow cathode lamp, so that only the background absorbance is measured. The difference between the 2 measured signals, when demodulated, produces a background corrected atomic absorption signal. Since the Perkin Elmer system measures the atomic absorption with the magnetic field off, and thus no splitting occurs, it experiences no decrease in the sensitivity for those elements exhibiting anomalous Zeeman splitting patterns. Both commercially available systems have provided viable background correction for atomic absorption spectrometry.

CHAPTER 3
THEORY OF COHERENT FORWARD SCATTERING ATOMIC SPECTROMETRY

Coherent forward scattering atomic spectrometry consists of the magneto-optic rotation of polarized light as it passes through an atomic vapor located within a transverse or longitudinal magnetic field, the Voigt effect and the Faraday effect, respectively. A second polarizer, the analyzer, is used to detect the amount of light which is rotated by the atoms. The coherent forward scattering signal consists of two effects, dichroism and birefringence. The system evaluated in this study is a Voigt effect coherent forward scattering atomic spectrometer and thus will be discussed in detail.

In a transverse magnetic field, the atomic absorption line splits into 3 components in a normal Zeeman splitting pattern, 1 π and 2 σ components, as discussed in Chapter 2 (see Figure 2). Associated with these absorbance lines are the anomalous dispersion functions, which also split in a magnetic field (see Figure 5). This figure reflects the increase and decrease in the refractive index which occurs at the wings of an absorbance line. The dispersion function is defined by the following equation (50):

$$n-1 = \frac{Ne^2f}{4\pi m\nu_0}\,\frac{\nu_0-\nu}{(\nu_0-\nu)^2+(\gamma/4\pi)^2} \qquad [18]$$

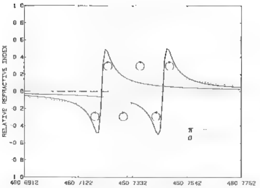

Figure 5 The Anomalous Dispersion Function for Sr at 460.7332 nm in a 2 T Magnetic Field Exhibiting a Normal Zeeman Splitting Pattern: S_0 ^1P transition

$$\gamma = 2\pi\Delta\nu_{1/2} = \text{damping term (Hz)} \qquad [19]$$

where n is the refractive index (dimensionless), e and m are the charge and mass of an electron, respectively, f is the oscillator strength, N is the number density of atoms per cm^3, ν is the frequency of light of interest (Hz), ν_0 is the resonance frequency of the absorbance line, and $\Delta\nu_{1/2}$ is the full width half maximum of the absorbance line (Hz). Substituting wavelength for frequency into Equation [18] results in the following equation:

$$n-1 = \frac{Ne^2 f\lambda_0}{4\pi mc^2} \frac{\frac{1}{\lambda_0} - \frac{1}{\lambda}}{(\frac{1}{\lambda_0} - \frac{1}{\lambda})^2 \; (\frac{\Delta\lambda_{1/2}}{2\lambda_0^2})^2} \qquad [20]$$

where λ_0 is the resonance wavelength of light (nm), λ is the wavelength of interest (nm), and $\Delta\lambda_{1/2}$ is the full width half maximum of the absorbance line (nm) In Figure 5, the anomalous dispersion function of the π component is represented by the dotted line and effects only light whose electric vector is oriented parallel to the magnetic field. The anomalous dispersion function of the σ components, the solid lines, effects only that light whose electric vector is oriented perpendicular to the magnetic field.

As was stated previously, the CFS signal is composed of a dichroic contribution, the difference in the absorption of the π and σ components, and a birefringent contribution, the difference between the refractive indices of the π and σ components. Through the use of models, the rotation of polarized light by the dichroism and the birefringence will be examined. Figure 6 represents the incident light, where the first polarizer, $\vec{E}$, is set at a 45° angle to the magnetic field, $\vec{H}$. The second set of axes in Figure 6 represents the movement of electric vector (the dashed arrow) through one period of oscillation, as represented in the bottom drawing. If the electric vector is projected back along the x and y axes, this represents the amount of light which is available to interact with the π and σ components, respectively (the solid lines in Figure 6).

A model of the dichroism, the difference between the absorbance of the π and σ components, is represented in Figure 7. Assume a line source is used which emits light at the resonance frequency, where only the π component can absorb (see Figure 2). Suppose a concentration of atoms that absorbs 50% of the light ($a(\pi)$=0.5, where a is the fraction absorbed) is present in the atom reservoir. This situation is represented in Figure 7 where 50% of the light along the x axis is absorbed (compare to Figure 6, where no absorption occurs). As can be seen in the model, the remaining light is rotated (the heavy dashed line). The analyzer, represented by the dotted line in the last axis, was set at a 90° angle to the first polarizer (compare to $\vec{E}$ in Figure 6). If the rotated vector is now projected onto the axis of the analyzer (the solid line in Figure 7), the amount of light passing through the analyzer is proportional to the amount of light which was absorbed. If this argument is extended to the σ components, an equal amount of light is rotated in the opposite direction. However, with a sufficient magnetic field, the π and σ

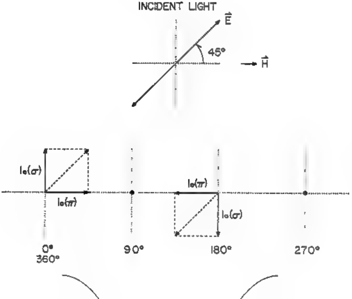

Figure 6. Model for the Incident Light in a Voigt Effect CFS Spectrometer

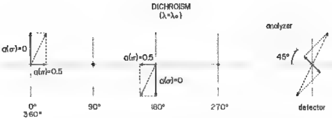

Figure 7 Model for the Dichroic Contribution to the CPS Signal in a Voigt Effect Spectrometer

components absorb at different wavelengths and since the analyzer is insensitive to the direction of rotation of the light, a dichroic signal will be produced over the entire profile of the atomic line (minus any overlap in the π and σ components, see Figure 8 as compared to Figure 2) when a continuum source is used. The dichroic signal of Sr at 460.7332 nm which exhibits a normal Zeeman splitting pattern is shown in Figure 8. It can be seen that all 3 components are completely resolved at the points where the π and σ components absorb an equal amount of light (see Figure 2), thus resulting in no rotation of the light. Since the σ components rotate the light in only 1 direction and the π component rotates the light in only the opposite direction, any anomalous Zeeman splitting which occurs will not reduce the sensitivity of the dichroic signal as long as the σ components remain fully resolved from the π components.

A model of the birefringence, the difference between the refractive indices of the π and σ components, is represented in Figure 9. Again assume a line source at the resonance frequency is used so that only interactions with the π component occur. The model in Figure 9 represents what will occur when the refractive index of the π component increases (see Figure 5). When the refractive index increases, the π component of the light will slow down with respect to the σ component which will remain unchanged. Assume an atom concentration is present which causes a phase shift of -90° in the π component of the light as represented in Figure 9. As can be seen from the model, the birefringence causes a conversion of the linearly polarized light to circularly polarized light, a portion of which can

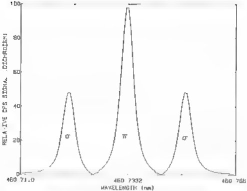

Figure 8. Profile of the Dichroism of Sr at 460.7332 nm in a 1.2 T Magnetic Field for a Voigt Effect CPS Spectrometer

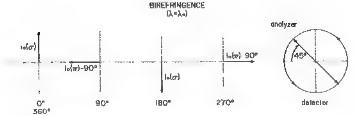

Figure 9 Model for the Birefringent Contribution to the CFS Signal in a Voigt Effect Spectrometer

pass through the analyzer (the solid line in the last axis in Figure 9). The assumption that a -90° phase shift occurs is an oversimplification. In real cases the phase shift will be smaller and a conversion to elliptically polarized light will occur. If this argument is extended to the σ components, a rotation in the opposite direction will occur with an increase in the refractive index. In Figure 5, the directions of rotation for the π (dotted line) and σ (solid lines) components are labeled. As can be seen in this figure, an increase in the refractive index of the π component causes the light to be rotated in the same direction as a decrease in the refractive index of the σ components. Also, an overlap of the σ and π components is not critical since a rotation in the same direction occurs. This is reflected in the birefringent profile for Sr at 460.7332 nm shown in Figure 10, which represents the difference in the refractive indices of the π and σ components. Again the analyzer is insensitive to the rotational direction of the light, producing a birefringent signal across the entire profile of the line. In Figure 10, the negative portion of the birefringent signal corresponds to an increase in signal intensity on a dark background which was produced by rotation of the light in the opposite direction, as is labeled. The birefringence, unlike the dichroism, however, can experience a reduction in sensitivity in the presence of anomalous Zeeman splitting. Since the anomalous dispersion function is bidirectional, any overlap between 2 split π components or 2 split σ components will result in destructive interference, eliminating the rotation of the light.

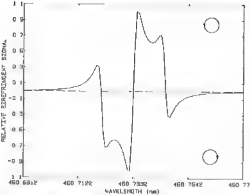

Figure 8 Profile of the Birefringence of Sr at 460.733 nm in a 2 T Magnetic Field for a Voigt Effect CFS Spectrometer

The intensity of the CFS signal passing through the analyzer for our system was derived (see Appendix) and is given by the following equation:

$$\begin{aligned} I_T = \frac{1}{2} I_0 \exp[-\frac{1}{2}(\alpha_x+\alpha_y)b]\{(\cos\theta\cos^2\phi+\sin\theta\cos\phi\sin\phi)^2 \cdot \\ \exp[\frac{1}{2}(\alpha_y-\alpha_x)b]+(\cos\theta\sin^2\phi-\sin\theta\cos\phi\sin\phi)^2\exp[\frac{1}{2}(\alpha_x-\alpha_y)b]+ \\ 2(\cos2\theta\cos^2\phi\sin^2\phi-\cos\theta\sin\theta\cos\phi\sin\phi\cos2\phi)\cos[\frac{\omega b}{c}(n_x-n_y)]\} \end{aligned} \qquad [21]$$

I_0 = intensity of incident light

α_x, α_y = Naperian absorption coefficient of π and σ components, parallel and perpendicular to the magnetic field, respectively, m^{-1}

n_x, n_y = refractive indices of the π and σ components, parallel and perpendicular to the magnetic field, respectively, dimensionless

b = pathlength, m

ω = angular frequency of the incident light, Hz

ϕ = angle between the axis of the first polarizer and the magnetic field, deg. or rad

θ = angle between the axes of the first polarizer and the analyzer, deg. or rad.

In most of the experiments in this study, the first polarizer was set at a 45° angle to the magnetic field ($\phi=45^\circ$) and the analyzer was set orthogonal to the first polarizer ($\theta=90^{\circ}$) reducing Equation [21] to the following:

$$I_T = \frac{1}{4} I_0 \exp[-\frac{1}{2}(\alpha_x+\alpha_y)b]\{\cosh[\frac{1}{2}(\alpha_x-\alpha_y)b]-\cos[\frac{\omega b}{c}(n_x-n_y)]\} \qquad [22]$$

By examining this equation, it can be seen that the CFS signal is proportional to the incident intensity of the light minus any overall absorption, including any molecular absorption, which would reduce the amount of light available to the π and σ components. The first expression in Equation [22] within the brackets corresponds to the dichroism term while the second expression corresponds to the birefringent term. Yamamoto et al. (15) and Kankare and Stephens (16) have derived the theory for the limiting cases. Kankare and Stephens make the assumptions that the absorption profile is Gaussian and $K_0C_ab<<1$ (where $K_0C_ab = \alpha_ab<<1$) reducing the general equation to the following equation which is applicable to the case of continuum excitation (16):

$$I_T = \frac{1}{128} I_0K_0^2C_a^2b^2(\{\exp[-(g-h)^2]+\exp[-(g+h)^2]-2\exp(-g^2)\}^2 \qquad [23]$$

$$+ \frac{4}{\pi}[\mathrm{daw}(g-h)+\mathrm{daw}(g+h)-2\mathrm{daw}(g)]^2)$$

when

$$g = d(\omega_0-\omega) \qquad [24]$$

$$h = d\Delta\omega_H \qquad [25]$$

$$\mathrm{daw}(x) = \exp(-x^2)\int_0^x \exp(z^2)dz = \text{Dawson's integral} \qquad [26]$$

$$K = K_0\exp[-(g\pm h)^2] = \text{molar Naperian absorption coefficient} \qquad [27]$$

$(2(\ln 2)^{1/2})d$ = full width half maximum of Doppler broadening

ω_0 = resonance frequency of the atom

ω = frequency of the incident light

$\Delta\omega_H$ = Zeeman shift

c_a = molar concentration of the analyte

b = path length

$\alpha = K_0C_a$

In the case of a line source (g=0), the equation can be further reduced (16) to the following:

$$I_T = \frac{1}{32} I_0K_0^2c_a^2b^2[\exp(-h^2)-1]^2 \qquad [28]$$

These equations demonstrate that when the analyzer is set orthogonal to the first polarizer the CFS signal which reaches the detector is proportional to the concentration squared.

The CFS signal can be linearized with respect to concentration by offsetting the analyzer by a small angle (16,18). This small offset angle, however, results in an increase the background by allowing some of the incident light to be transmitted through the polarizers. Stephens and Kankare (16) have derived the equation for the linearized CFS signal using a line source to be the following:

$$I_T = \frac{1}{2}\sin^2\theta' + \frac{1}{8}\sin 2\theta'[\exp(-h^2)-1]K_0 c_a b l I_0 \qquad [29]$$

$\theta' = 90^\circ + \theta$ = offset of the polarizers from being orthogonal, restricted to small offset angles.

As the equation reflects, the CFS signal becomes linearized with respect to concentration when small offset angles are employed, the optimum offset angle being 8.5° as experimentally determined by Kankare and Stephens (18).

CHAPTER 4
EXPERIMENTAL

The basic experimental set-up of a CFS spectrometer consists of an excitation source, 2 polarizers, a magnet, and a detection system. A block diagram of the experimental set-up used to study the noise characteristics of CFS is given in Figure 11. A 300W Eimac (Varian Instruments, 611 Hansen Way, Palo Alto, CA 94303) xenon arc lamp was used as an excitation source in the experimental system. The continuum source was focused through a pinhole aperture and recollimated by a second lens. The light beam then passed through a Photon Technologies International (P.O. Box AA, Princeton, NJ 08542) chopper which was operated at 467 Hz, an IR filter, and then through the first of a pair of Karl Lambrecht (4204 N. Lincoln Ave., Chicago, IL 60618) calcite Glan-Faucault prism polarizers which was oriented at a 45° angle to the magnetic field. The magnet consisted of a Varian (611 Hansen Way, Palo Alto, CA 94303) V-6060 magnet system from an A-60 NMR which was modified to produce a variable DC magnetic field up to 1.4 T. A 1.2 T field was employed for the study. A fuel-rich air-acetylene flame served as the atom reservoir. The burner was a laboratory constructed titanium 3" slot burner with 2 side slots for an argon sheath. After passing through the magnet, the light beam passes through the second polarizer, the analyzer, which was oriented either orthogonal to the first polarizer or at an 8.5° offset angle

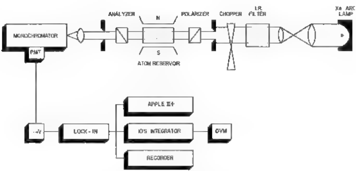

Figure 11   Block Diagram for the Multi-Element CFS Spectrometer

from this (Q=98.5), to evaluate the squared and linear systems, respectively. The light beam then passed through a 1/2" aperture (to match the f-number of the monochromator) and was focused by a 3" lens into a Shoeffel-McPherson (530 Main St., Acton, MA 01720) EU700 monochromator, equipped with a Hamamatsu (420 South Ave., Middlesex, NJ 08846) R212UH photomultiplier tube. A Keithley (28775 Aurora Rd., Cleveland, OH 44139) 244 High Voltage Power Supply was used to power the PM tube at −960 V. A slit width of 130 μm, which corresponds to a spectral bandpass of 0.29 nm, was used as it corresponded to the optimum signal to noise ratio.

Several different detection systems were used to examine the primary noise sources for the system. Background spectra of the flame were run with the chopper off and the PM tube output going straight to the Fisher Scientific Co. (P.O. Box 13430, Orlando, FL 32809) Model 5000 strip chart recorder. All other background spectra were measured with the chopper on. In this case, the PM tube output was amplified by a PAR model 181 current-to-voltage amplifier and demodulated and filtered by a PAR (EG&G PAR, P.O. Box 2566, Princeton, NJ 08540) model 186A lock-in-amplifier with an output time constant of 0.3 s. The output of the lock-in-amplifier was then sent to a strip chart recorder. Noise power spectra of the squared and linear systems were measured with a Wavetek (10 Volvo Dr., Rockleigh, NJ 07647) Cross-Channel Spectrum Analyzer Model 5820B. Since the Spectrum Analyzer was not accurate down to DC signals (0 Hz), amplitude modulation was used to move the signal and any associated noise up into a useful range for the Spectrum Analyzer. To measure the noise power spectra, the output of the current to voltage converter was sent to the Spectrum Analyzer directly which took the average of 256 spectra.

Limits of detection (LODs) were also run for the systems using amplitude modulation and DC measurement. In the case of amplitude modulation, the output of the PM tube is again sent to the current to voltage amplifier and into the lock-in amplifier. A time constant of 1 s was used on the output of the lock-in amplifier which was filtered with a laboratory constructed 10 s integrator and sent to a Keithley model 175 digital multimeter. When DC measurements were made, the chopper was turned off and the above detection system was used with the exception of the removal of the lock-in amplifier from the circuit.

A block diagram of the laser-excited CFS system is given in Figure 12. The laser system which was used consisted of a Molectron (Cooper Laser Sonics, Laser Products Div., 928 E. Meadow Dr., Palo Alto, CA 94303) Model UV24 nitrogen laser pumping a Molectron DLII tunable dye laser (bandwidth of 0.3 nm). A beam splitter was used to monitor the output of the nitrogen laser to a photodiode which was used to trigger the boxcar. Inrad (Interactive Radiation Inc., 181 Legrand Ave., Northvale, NJ 07647) doubling crystals were used to double the fundamental of the dye laser when necessary. The output of the dye laser was recollimated before being sent to the experimental set-up. Neutral density filters (ND) were used prior to the first polarizer in some instances. An aperture was placed before the first polarizer to minimize uncollimated light. The polarizers, set in an orthogonal orientation, the magnet and the flame were the same as

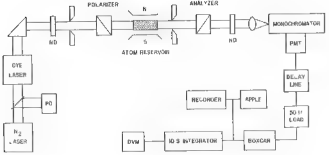

Figure 2 Block Diagram for the Laser-Excited CFS Spectrometer

described for the previous study. A graphite furnace was also used as an atom reservoir in this study. The graphite furnace consisted of laboratory constructed brass electrodes with a quartz sheath and quartz end windows and contained Ringsdorf (Sigri Corporation, P.O. Box 922, Sommerville, NJ 08876) pyrolytically coated graphite tubes (6 mm o.d. x 4 mm i.d. x 3" long). The furnaces were heated in an argon atmosphere, with the exception that the argon flow to the inside of the tube was turned off during atomization. A second aperture was placed prior to the analyzer to reduce emission from the flame or furnace, which is incoherent unlike the CFS signal. The monochromator was equipped with a Hamamatsu 928 PM tube, which was wired for fast response. A slit width of 200 μm, which corresponded to a spectral bandpass of 0.44 nm, was used. The PM tube was powered at -1000 V.

The signal from the PM tube was sent through an Allen Avionics switch variable delay line, Model V127Z050, and a 50Ω load into a Stanford Research Systems (460 California Ave., Palo Alto, CA 94303) Model SR250 gated integrator and boxcar averager. The averaged output of 3 shots was then sent to the 10 s integrator and a digital voltmeter in the case of the flame. When the graphite furnace was used, the output of the boxcar was sent to the strip chart recorder, for a hard copy, and to the Interactive Structures (P.O. Box 404, Bala Cynwyd, PA 19004) AI13 Data Acquisition System into an Apple (10260 Brandley Dr., Cupertino, CA 95014) II+ computer, which was used to integrate the peak area of a 5 μL sample. The Apple computer was also used to program the Electronic Measurements (405 Essex Rd., Neptune, NJ 07753) Model SCR20-250 5kW furnace power supply. Two Apple Disk II

Disk Drives and a Leedex video 100 monitor completed the computer system.

Figure 11 is also a block diagram of the system used to evaluate the analytical figures of merit for the multi-element CFS system. The experimental set-up is the same as that described in the system used to characterize the noise, with some minor modifications. A Hamamatsu 928 PM tube powered at -1000 V was used in place of the Hamamatsu R212UH PM tube. All other parameters were identical to that previously described for measuring LODs using amplitude modulation. A graphite furnace was also used as an atom reservoir as was discussed in the laser-excited CFS system. When the furnace was employed, the aperture prior to the lens which focused the light into the monochromator was reduced to 1/6" (4 mm) to match the i.d. of the furnace. The 3" lens was then replaced by a 1" lens to match the f-number of the monochromator. A prior multi-element system (the old system) was also evaluated using a smaller ANAC (GMW Associates, 1060 Lakeview Way, Redwood City, CA 94062) 1.75" electromagnet which could only produce a 0.7 T magnetic field when the flame was used. The burner used was a brass laboratory constructed slot burner made to fit the physical dimensions of the smaller magnet. The graphite furnaces used in this previous study were Ultra Carbon (P.O. Box X-747, Bay City, MI 48707) high density, high purity graphite tubes (6 mm o.d. x 4 mm i.d. x 3" long). Other than the changes in the magnet and the atom reservoirs, the system was unchanged.

Stock solutions of 1000 mg/L were prepared by dissolving the pure metals or reagent grade salts in a minimum amount of acid and then diluting with deionized water ($\approx$12 MΩcm^{-1} resistivity). volumetric dilutions were made to obtain the desired standard concentration. In many cases, the stock solutions and standards used with the furnace were made and diluted with 10% nitric acid which had been sub-boiling distilled.

CHAPTER 5
NOISE CHARACTERISTICS OF A VOIGT EFFECT CFS SPECTROMETER

Many reviews and studies have been published on the signal to noise characteristics of both atomic fluorescence spectrometry (AFS) and AAS (51-57), while only one study has appeared on the signal to noise characteristics of CFS (19). An analysis of the noise characteristics of CFS can provide useful information for the design and optimization of a Voigt effect CFS system. It is particularly useful when evaluating the squared vs linear CFS systems.

Background spectra of the different components of the system were recorded to evaluate their relative contributions to the signal. A DC spectrum of the background emission from the fuel-rich air-acetylene flame is shown in Figure 13. At 200 nm, the spectrum is flat because the calcite polarizers cut off at 214 nm. The analyzer also reduced the emission from the flame seen by the detector by a factor of 2 and the apertures after the flame reduced the solid angle and thus the emission from the flame seen by the detector. Two bands can be seen on top of the background emission from the flame at 306 nm and 612 nm. These bands are the OH emission bands. The 612 nm band is the second order band at 306 nm which disappears when a 500 nm sharp cut filter is placed after the excitation source. The broad background is due to the spectral response of the monochromator and PM

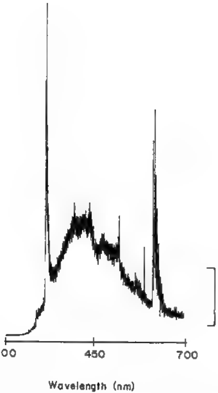

Figure 13. Background Spectrum for the Fuel Rich Air-Acetylene Flame

tube and the black body radiation from the fuel-rich air-acetylene flame. It was necessary to run the flame very fuel-rich to minimize the loud audible oscillation of the burner and the aluminum pole caps which protect the faces of the magnet poles from the flame. The design of a new burner allowing more adjustment of the fuel-to-oxidant ratio would help to reduce this background.

All other background spectra were taken using a lock-in amplifier and a chopper to correct for the background emission from the flame. The background spectra of the lamp for the squared system with crossed polarizers are shown in Figure 14. The bottom spectrum (b) is a spectrum of the lamp alone. If the lamp spectrum is compared to the flame emission (see Figure 13), it can be seen that the emission from the flame is about an order of magnitude larger than the light getting through the crossed polarizers. The dark current on the PM tube is also about the same order of magnitude as the flame emission. The top (a) spectrum in Figure 14 shows the lamp with the flame on. As can easily be seen from the spectrum, the lock-in amplifier corrects for the emission signal from the flame and the dark current signal from the PM tube. The shot noise from the emission and the dark current are still evident on this spectrum, however. If the magnet is turned on (1.2 T field) and Sr is aspirated into the flame, the spectrum shown in Figure 15 is obtained. Again 2 bands are seen at 306 nm and 612 nm. These bands, which are a factor of 5 times larger than the emission bands (see Figure 13), are due to the rotation of the light by the OH in the flame. The band at 612 nm is again second order of the OH band at 306 nm and can be corrected by using a sharp cut filter

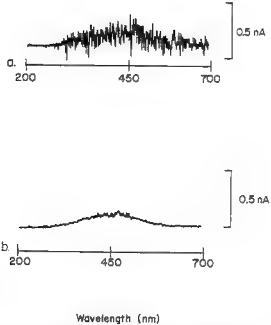

Figure 14. Background Spectra for the Xenon Arc Lamp Through Crossed Polarizers Using a Lock-in Amplifier With (a) and Without (b) the Flame On

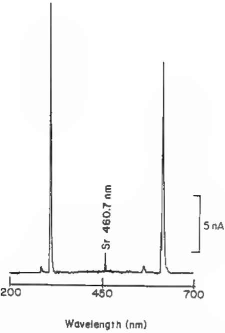

Figure 15 The Background Spectrum for the Squared CFS System ($\theta = 90°$)

to remove the 306 nm light. These OH bands appear due to the Zeeman splitting of diatomic molecules in a magnetic field (57) and the high concentration of OH in the products of the flame (1-2%, 58). Thus the OH bands at 306 nm will prove to be a spectral interference in CFS as in AFS and AAS. Since most elements do not have lines in this region, this does not severely limit the technique. It should also be noted that when the graphite furnace is used as the atom reservoir, the sample is dried prior to atomization thus eliminating any problems with spectral interference from the OH bands.

A background spectrum for the linear system with polarizers offset by an 8.5° angle ($\theta=98.5^\circ$) is given in Figure 16. In this spectrum the lamp, flame, and magnet are on. It can be seen that the light getting through the polarizers, now that they are offset, is approximately 3 orders of magnitude larger than the light getting through the crossed polarizers (see Figure 14), at the center of the spectral range ($\sim$450 nm). It should also be noted that the amount of light getting through the polarizers is approximately 1 order of magnitude larger than the signals produced by OH in the squared system (see Figure 15). Thus it can be seen that in going from the squared to the linear system, the primary source of noise has changed from the emission of the flame and the dark current of the PM tube to the source light transmitted through the non-orthogonal polarizers. The manner in which the noise characteristics are changed in going from the squared to the linear system will be evaluated using the noise power spectra of the systems.

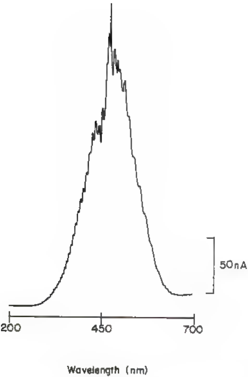

Figure 16. The Background Spectrum for the Linear CFS System (θ = 98.5°)

The noise power spectrum of the squared system is given in Figure 17. All noise power spectra were taken using the OH band at 306 nm so that only the blank was aspirated into the flame. The first peak at ~13 Hz is a component of the flame and can be seen in a spectrum taken of only the flame. The flame also has flicker noise (1/f noise) which falls off rapidly at low frequencies (<20 Hz). There is also a component at ~90 Hz which was electronic noise from the current to voltage amplifier. The main peak, however, can be seen at 467 Hz, the chopping frequency. This peak and the 2 peaks on either side of it disappear when the magnet is turned off and, therefore, are due entirely to the signal. The 2 peaks at either side of the signal peak are at ±13 Hz from the chopping frequency and are, therefore, attributed to the flame. It would thus appear that the 13 Hz component of the flame is a multiplicative noise which moves up with the signal in some manner. It should be noted that with the use of a lock-in amplifier and a sufficiently long time constant the signal peak should be resolved from this multiplicative noise from the flame. This noise power spectrum also shows some white noise at a level of ≈-97 $dBV/(Hz)^{1/2}$ around the signal peak.

A comparison of the noise power spectra of the squared system and the linear system is also of interest. The noise power spectrum for the linear system (θ=98.5) with the magnet off (dashed line) and on (solid line) are shown in Figure 18. The main peak still appears at 467 Hz but is only 2.3 $dBV/(Hz)^{1/2}$ greater with the magnet on than off. The wings of this peak are also broadened due to flicker noise from the Eimac xenon arc lamp, which is modulated and thus moves up

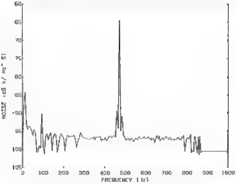

Figure 17 The Noise Power Spectrum for the Squared CFS System Taken at 306 nm

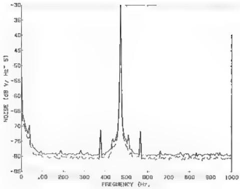

Figure 18 The Noise Power Spectra for the Linear CFS System Taken at 306 nm

with the signal. A spectrum taken of the lamp only shows the flicker noise of the lamp does not fall off until ~50 Hz. The 2 peaks on either side of the main peak at ±~94 Hz are present when the magnet is on and off and are, therefore, associated with the source. The other 2 peaks around the 467 Hz peak are at ±37.5 Hz. There is also a small component at 37.5 Hz, which is attributed to the flame. The flame appears to have some drift over time so that the frequency of oscillation can change. Thus, it would appear this 37.5 Hz peak corresponds to the 13 Hz peak in the squared system (see Figure 17) and is a multiplicative noise associated with the signal. Another point of interest is that the white noise for the linear system with the magnet on is ≈-79 dBV/(Hz)$^{1/2}$ or 18 dBV/(Hz)$^{1/2}$ (almost 1 order of magnitude) higher than the white noise in the squared system.

Thus it would appear that the noise characteristics of the squared vs the linear system are quite different. For the squared system, with the emission from the flame as the predominate noise source, it may be advantageous to use amplitude modulation to move the CFS signal out of the flicker noise of the flame at low frequencies. Although some of the noise from the flame moves up with the signal, it is possible with the use of the lock-in amplifier and a sufficient time constant to separate the signal from these outer peaks (see Figure 17). A second advantage in using amplitude modulation and lock-in measurement over DC measurement can be seen in the curve of growth for the DC measurement of Ca at 422.673 nm in Figure 19. The AES curve of growth has a slope of 1.05 (r=0.9995), the CFS curve of growth has a slope of 2.006 (r=0.9996) and the CFS + AE curve of

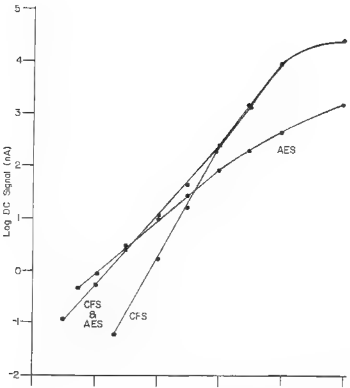

Figure .9 CFS and AES Curves of Growth for Ca at 422.673 nm With the Squared CFS System Using a DC Measurement System

growth has a slope of 1.30 (r=0.95). When the curve of the Atomic Emission (AE) is compared to the CFS curve, it can be seen that the AE signal predominates at the lower concentrations while the CFS signal predominates at higher concentrations. When a DC measurement system is used to measure the CFS signal in a squared orientation ($\phi=90^{\circ}$), some care must be taken to correct for the atomic emission which is linear with concentration not squared. By using amplitude modulation, the emission is automatically subtracted out leaving the corrected CFS signal. The linear system ($\theta=98.5^{\circ}$, does not have this problem, however. Since the CFS signal and the AE signal are linear in terms of concentration, a calibration curve may be made using the sum of the AE and CFS signals. Amplitude modulation for the linear system, however, does not appear advantageous. Since the predominate noise source in the linear system is the light from the source being transmitted through the polarizers, chopping the light only serves to move the flicker noise up with the CFS signal. Other types of modulation schemes, as an AC magnet or wavelength modulation, could prove advantageous in that they could correct for the flicker noise of the source, since it is viewed during both half cycles of modulation.

To further compare AM vs DC measurements, limits of detection (LODs) were determined for both using the squared orientation ($\theta=90^{\circ}$) and the linear orientation ($\theta=98.5^{\circ}$). The LODs for Ca at 422.673 nm are given in Table 2. The LODs were calculated by taking 3 times the standard deviation of 16 blank readings, dividing by the slope of a plot of concentration squared vs CFS signal, and then taking the square root of the result. All calibration curves used in calculating

Table 2. LIMITS OF DETECTION IN mg/L (S/N = 3) FOR CA AT 422.673 nm USING AMPLITUDE MODULATION (AM) VS. DC MEASUREMENT

	MEASUREMENT SYSTEM	
POLARIZER ORIENTATION	AM	DC
Squared System ($\theta = 90°$)	0.2	0.2
Linear System ($\theta = 98.5°$)	1.	1.

LODs had a correlation coefficient of at least 0.999. The results in Table 2 indicate no significant difference between AM and DC measurement for either the squared or linear systems. The LODs for the squared system are, however, better than those for the linear system. This, however, might be changed if a different modulation system was used in the case of the linear system. The LODs of the squared system could be improved by increasing the intensity of the incident light. This would increase the CFS signal while increasing the amount of light being transmitted through the crossed polarizers so that it is at least of the same magnitude as the emission from the flame. Thus, the study of the noise characteristics of the linear and the squared CFS systems has helped enumerate the various problems which will be encountered in both systems.

CHAPTER 6
LASER-EXCITED CFS

The use of both pulsed and continuous wavelength (CW) lasers as an intense excitation source for AFS has been shown to be analytically useful especially for trace analysis (60-64). Theoretical studies of CFS have shown that the signal is proportional to the incident intensity of the light (11-20, as it is in AFS. Because of this relationship and the zero background, it was postulated that laser-excited CFS might be a viable analytical technique. Also since the CFS signal consists of the incident light which has been rotated, the coherent properties of the laser beam might also prove advantageous. A squared system ($\theta=90^{\circ}$) was used, because linearization ($\theta=98.5^{\circ}$) causes an increased background, which was considered unfavorable in the case of laser excitation.

A curve of growth for Na at 588.995 nm is given in Figure 20. As can be seen from this curve, the CFS signal increases with a log-log slope of 2.05, reflecting the signal's dependence on the square of the concentration. The CFS signal is linear over 3 orders of magnitude in concentration. The curve also shows a decrease at high concentration which is probably due to broadening of the absorption line. Broadening of the σ and π components causes overlap in the wings of the absorption line resulting in a decrease in both the dichroism and

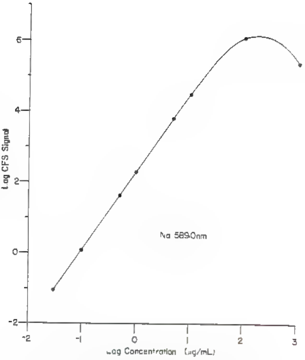

Figure 20. CFS Curve of Growth for Na at 589.0 nm in a Flame Using Laser Excitation

the birefringence. This effect can be minimized by increasing the magnetic field so that the σ and π components are further separated. This was not possible in our case, however, since the maximum magnetic field was employed. The shape of the calibration curve should start to level off, due to a plateau in the absorption coefficients at high concentration, before the decrease in the CFS signal due to broadening.

A log-log calibration curve of the CFS signal for Sr at 460.7332 nm vs the spectral irradiance of the laser is shown in Figure 21. This curve demonstrates that the intensity of the CFS signal is proportional to the incident intensity of the laser light (log-log slope of 0.96). As saturation occurs, dichroism decreases, causing the CFS signal to level off as seen in the plot. There is also a negative slope exhibited at higher powers. This decrease may be explained by saturation broadening (65,66). Broadening causes overlap of the σ and π components which decreases the birefringent signal, while saturation causes the net absorption coefficient to approach zero which decreases the dichroism, therefore increasing the intensity of the excitation source causes an increase in the CFS signal up to the point where saturation occurs.

While the use of lasers as an excitation source provided useful theoretical information, it did not prove to be analytically useful as reflected in the limits of detection given in Table 3. These results are poor compared to those obtained using hollow cathode lamps and xenon arc lamps (21,23,24,26,27,29,67) with the exception of Sr at 460.7332 where the best laser dye for the nitrogen laser is used. The use of the laser increased the CFS signal; however, the noise

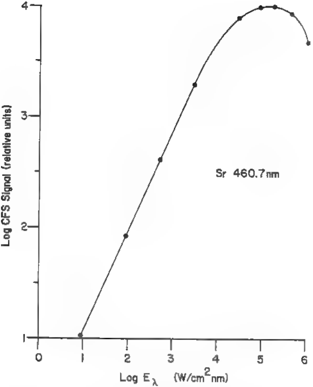

Figure 2. Plot of the Laser Intensity vs. the CFS Signal in a Flame

Table 3 LIMITS OF DETECTION (S/N = 3) FOR LASER EXCITED CFS

ELEMENT	WAVELENGTH (nm)	FLAME (mg/L)	FURNACE (ng)[a]
Ca	422.673	0.3	
In	303.936	1	
Mg	285.213	0.1	–
Na	588.995	0.03	
Pb	283.306	–	5
Sr	460.733	0.09	2

a) Absolute detection limits in the furnace are based on an injection volume of 5 μL increased disproportionately. The primary source of noise was the amount of light which passed through the crossed polarizers due to their imperfect extinction ratio. It was found that as the laser power increased over 4 orders of magnitude, the extinction ratio decreased by an order of magnitude. The shot to shot noise and the pointing noise are the major noise sources seen on the laser light which was transmitted through the polarizer. It was also discovered that the end windows on the furnace were birefringent increasing the blank signal and thus lowering the LODs for the furnace. This problem was corrected at a later date. Thus despite the increased intensity of the light, the pulsed laser proved to be too noisy to be an analytically useful source for CFS. While a CW laser may provide better results due to its stability, it has a limited wavelength range and therefore would be less useful analytically.

The use of a tunable pulse dye laser as an excitation source for CFS proved to be too noisy despite its high intensity; therefore, a poorer signal-to-noise ratio was observed. This study did, however, show that if an insufficient magnetic field is used the linear dynamic range of the technique may be decreased due to overlapping of the σ and π components. The CFS signal may be increased by increasing the incident light up to the point where optical saturation occurs. Thus, the future of CFS as an analytical technique will not likely include lasers as excitation sources. However, continuum sources have been shown to be analytically useful in multi-element analysis (26-29).

CHAPTER 7
MULTI-ELEMENT CFS

The use of a continuum source as an excitation source for AAS (68,69) and AFS (70-73) has been shown to be analytically useful. A continuum source has also been shown to be a viable light source for CFS (26-29). The use of a continuum source in CFS allows for excitation of the entire profile of the split atomic line. The multi-element capabilities of CFS can also be evaluated, since all atomic transitions are excited simultaneously.

A curve of growth measured with the new system (using the Varian magnet) for Na at 589.0 nm in a flame is given in Figure 22. The log-log slope of the curve is 2.006 which reflects that the CFS signal is dependent on the square of the concentration, with a correlation coefficient of 0.99994. It should be noted that the shape of the continuum-excited curve of growth for Na is identical to the laser-excited curve of growth for Na (see Figure 20). This further confirms that the negative slope exhibited at higher concentration is probably a result of broadening and overlap in the π and σ components and is not dependent on the profile of the source. Figure 23 shows the curve of growth for Ca at 422.673 nm in a flame measured with the old system (see Chapter 4, Experimental). The log-log slope of this curve is 1.97 (r=0.9997), again reflecting the CFS signal is dependent on the square of the concentration. In examining these calibration

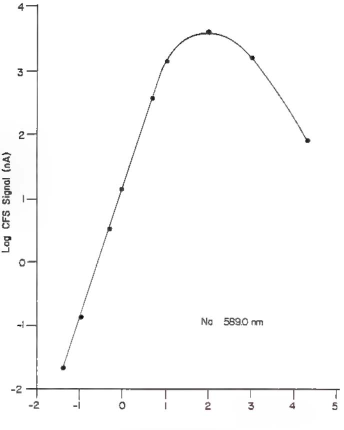

Figure 22. CFS Curve of Growth for Na at 589.0 nm in a Flame Using Continuum Excitation

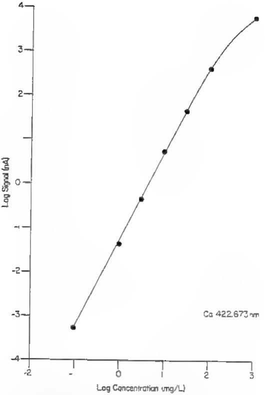

Figure 23. CFS Curve of Growth for Ca at 422.673 nm in a Flame Using Continuum Excitation

curves it can be seen that the CFS signal for Cu is a straight line (with a slope of 2) over 3 orders of magnitude while the signal for Na has a useful analytical range (LDR) over 2.5 orders of magnitude. A curve of growth for Cu at 324.754 nm in a furnace (in the old system) is given in Figure 24. The log-log slope of this calibration curve is 1.90 (r=0.9996). The linear dynamic range of the CFS signal using the furnace is slightly under 2 orders of magnitude. The LDRs of most elements in the flame is approximately 2-4 orders of magnitude, while the LDRs for the furnace are approximately 1-3 orders of magnitude. The reason for the reduced LDRs seen in the furnace is due to the inability of the furnace to atomize high concentrations of solids and changes in the atomization conditions in the presence of high concentrations of solids.

Table 4 lists the limits of detection (LODs) (S/N=3) for several elements in both the old (the values in parentheses) and the new systems. The LODs were calculated by taking 3 times the standard deviation of 16 blank readings, dividing by the slope of a plot of the CFS signal vs the concentration squared and taking the square root of this value. The LODs reflected in Table 4 are in many cases detectable amounts which can be measured in real samples and in some cases are real points on the calibration curves. The LODs of the flame are still rather poor to be of use in trace analysis. The LOD's of the furnace are, however, more promising. The LODs for CFS in the furnace are approximately 1 to 2 orders of magnitude worse than those obtained using ZAAS (8). It should also be noted that an improvement in the LODs of the new system was obtained over the old system. This

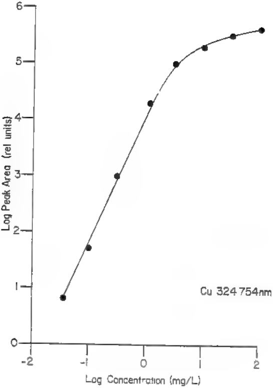

Figure 24. CFS Curve of Growth for Cu at 324.754 nm in a Graphite Furnace Using Continuum Excitation

Table 4 LIMITS OF DETECTION (S/N = 3) FOR MULTI-ELEMENTS CPS

ELEMENT	WAVELENGTH (nm)	FLAME (mg/L)	FURNACE (ng)^{a}
Ca	422.673	0.1 (0.7)^{b}	
Cr	357.869	3 (6)^{b}	–
Cu	324.754	0.2	0.3 (0.5)^{b}
Pb	283.306	3	3
Mg	285.213	0.05 (0.2)^{b}	–
Mn	279.482	– (1)^{b}	–
Ag	328.068	0.3 (3)^{b}	0.1
Na	588.995	0.04	0.04
Sr	460.733	0.6	0.2
Tl	377.572	2	

a) Absolute detection limits in the furnace are based on an injection volume of 5μL

b) All values in parentheses are for the old system using the smaller ARAC magnet is due to the use of the larger Varian magnet which produces a constant magnetic field over the entire pathlength of the flame and furnace. The Varian electromagnet also allowed a magnetic field of 1.2 T to be used with the flame while the ANAC electromagnet produced a magnetic field of 0.7 T with the flame. This increase in the magnetic field should fully separate the σ and π components over the entire pathlength of the atom reservoir, thus enhancing the CFS signal.

The LODs of the present system would be greatly improved by using a more intense source which has better optical qualities. It would be advantageous to increase the source intensity to the point that the blank (the light getting through the crossed polarizers) was increased sufficiently to be of the same order of magnitude as the flame emission or the dark current from the PM tube. The LOD for Pb at 283.306 nm could be decreased by the use of quartz polarizers, which would also allow the evaluation of Zn and As at 213.856 nm and 197.2 nm, respectively.

While the LODs for the CFS system are still poor compared to those found in AAS, the multi-element capabilities of the system still make the system analytically viable. The future of CFS in analytical chemistry lies in the evaluation of a simultaneous multi-element furnace system. The furnace has the advantage of handling small sample sizes and providing low absolute detection limits. The CFS also has the advantage of being a background corrected technique. Thus with a further reduction in the LODs, CFS will become a viable analytical technique for multi-element analysis.

CHAPTER 8
THE FUTURE OF CFS IN ANALYTICAL CHEMISTRY

Much work remains to be done in evaluating CFS as an analytical technique. One area of interest would be in the evaluation of different excitation sources for CFS. Both hollow cathode lamps and xenon arc lamps have been evaluated as excitation sources (21-29). Development of a new continuum source with better optical quality would be advantageous. Klueppel and Walters (74) found that, when a magnetic field is placed around a spark discharge or plasma (a theta pinch spark or plasma), an increased collision frequency causes an increase in the background continuum. The use of a theta pinch plasma as a source for CFS might prove interesting. If a miniature plasma torch could be designed to fit inside the poles of a DC magnet, perhaps the background continuum of the plasma could be increased to a point where it could be used as a source. If no nebulizer is used, the stability of the plasma should be increased. The optical quality of the light beam should also be better, since no electrodes are in the profile of the beam. The theta pinch plasma as a source also has the advantage of having an infinite lifetime.

Another area of interest would be the use of laser-excited CFS to evaluate the effect of saturated absorbance on the CFS line profile. When the absorbance profile becomes saturated, the absorbance will go to zero (75,76). By examining the equation for the intensity of the CFS signal (see Equation [21]), it can be seen that when the absorbance is saturated only the birefringent portion of the CFS signal should remain. An argon ion laser could be employed to saturate the absorbance of Na at 589.0 nm. If an interferometer is used to scan over the line profile, the effect of saturation on the birefringent signal can be evaluated. Thus the relationship between dichroism and birefringence can be experimentally evaluated.

An evaluation of wavelength modulation and an AC magnet could also provide interesting information. Wavelength modulation by necessity involves the measurement of atomic emission. Due to this, wavelength modulation may be employed only in a linear system (θ=98.5^o), where the AE+CFS signal can be used to construct a linear calibration curve. Wavelength modulation will, however, correct for the source light which passes through the uncrossed polarizers along with background emission from the flame. An AC magnet, however, may be used for a linear and a squared system. An AC magnet would allow correction for any source light transmitted through the polarizers, the flame background emission and the atomic emission. Thus, an AC magnet may prove to be the most advantageous modulation scheme for CFS, as it is for many elements in ZAAS (49).

The most interesting study, however, would be in the design and evaluation of a simultaneous multi-element ZAAS/CFS spectrometer. As was explained earlier (see Chapter 2), the Perkin Elmer ZAAS system employs an AC magnet and so the sensitivity of those elements experiencing anomalous Zeeman splitting is not reduced (49). The multi-element ZAAS/CFS system will also employ an AC magnet. A continuum source will be used to excite simultaneously all the atom transitions. A direct reader echelle spectrometer, which has been modified so that demodulation of a signal is possible, will be used. If the spectral bandpass of the echelle polychromator is of the same order of magnitude as the line width of a hollow cathode lamp, multi-element ZAAS should be possible. In the ZAAS mode, only one polarizer set perpendicular to the magnetic field will be used to measure the absorbance of the σ components. When the magnet is off and no splitting occurs, the atomic absorbance plus background absorbance is measured. When the magnet is on, the σ components should be split outside of the spectral bandpass of the spectrometer and only background absorbance is measured. Demodulation should result in a background-corrected atomic absorption signal. The system can also be set up as a simultaneous multi-element CFS system with the addition of a second polarizer. The first polarizer should be placed prior to the atom reservoir and oriented at a 45° angle to the magnetic field, while the second polarizer is placed after the atom reservoir and oriented orthogonal to the first polarizer or offset by an 8.5° angle. By using this system, a fair comparison may be made of ZAAS and CFS. It would also be of interest to evaluate real samples and compare the background correction capabilities of both systems.

CHAPTER 9
CONCLUSIONS

In conclusion, CFS is emerging as a new elemental technique in analytical chemistry. When compared to AAS and AFS, CFS has some advantages. Both CFS and AAS produce coherent signals, unlike AFS. Due to coherence, an increase in the distance between the atom reservoir will decrease the emission from the atom reservoir while the signal remains unchanged. However, CFS is a zero background technique, as is AFS. Thus, the limiting noise in CFS should be smaller than in AAS, where the source is viewed. In being an absorbance process, CFS also is not limited by a quantum efficiency as in AFS. The main disadvantage in CFS is the quadratic dependence of the signal on the concentration. This has a detrimental effect on the LODs for CFS. It remains to be seen, however, how these factors will affect the future of CFS in the field of atomic spectrometry.

This study has served to establish the noise characteristics of a Voigt effect CFS system, which will prove valuable in the design of future systems. The study of laser-excited CFS has shown that pulsed lasers are unsuitable sources for CFS. However, the use of a continuum source has been shown to be analytically viable, especially when a furnace is used as an atom reservoir. Thus, this study serves as a basis for the further evaluation and improvement of a CFS system as an analytical tool for multi-element analysis.

APPENDIX I
THE DERIVATION OF A GENERAL EQUATION FOR A VOIGT EFFECT CFS SPECTROMETER

The use of Jones calculus allows for the evaluation of a train of optical components by taking the products of their representative matrices. Thus, the following equation represents the set-up of a Voigt effect CFS spectrometer based on the work done by Kankare and Stephens (16).

$$A = R_{\theta} P_y R_{\theta}^T R_{\phi} V R_{\phi}^T P_x \qquad [30]$$

where P_x and P_y are the polarizers which are located before and after the atom reservoir, respectively, V is the matrix for the Voigt effect, and R_x is a rotational matrix which orients the axes of two optical components. The following matrices are used in equation [30], with θ representing the angle between the two polarizers and φ representing the angle between the first polarizer and the magnetic field

$$R_x = \begin{vmatrix} \cos x & -\sin x \\ \sin x & \cos x \end{vmatrix} \qquad [31]$$

where x represents the angle between the two components and R_x^T is the transpose of the matrix. The polarizer and the analyzer, P_x and P_y respectively, were represented by the same matrix so that θ represents the angle between the axes of the two polarizers. They were also assumed to have a perfect extinction ratio which is an oversimplification.

$$P_x = P_y = \begin{vmatrix} 1 & 0 \\ 0 & 0 \end{vmatrix}, \qquad [32]$$

The matrix which represents the Voigt effect is the following (16)

$$V = \begin{vmatrix} \exp[i(\hat{n}_x - 1)\frac{\omega b}{c}] & 0 \\ 0 & \exp[i(\hat{n}_y - 1)\frac{\omega b}{c}] \end{vmatrix} \qquad [33]$$

where $\hat{n}_x$ and $\hat{n}_y$ are the complex refractive indices of the π and σ components, respectively, ω is the angular frequency of the incident light, b is the pathlength and c is the speed of light in a vacuum. The intensity of the light transmitted through the polarizers is represented by the following equation:

$$I_T = \tfrac{1}{2} I_0 \mathrm{Tr}\{[A]^* [A]\} \qquad [34]$$

where I_0 is the intensity of the incident light, Tr stands for the trace of the product, and $[A]^*$ is the complex conjugate of the transpose of [A].

Upon multiplication of these matrices, the matrix A was determined to be represented by the following matrix.

$$A = \begin{vmatrix} (\cos^2\theta\cos^2\phi+\cos\theta\sin\theta\cos\phi\sin\phi)X+(\cos^2\theta\sin^2\phi-\cos\theta\sin\theta\cos\phi\sin\phi)Y & 0 \\ (\cos\theta\sin\theta\cos^2\phi+\sin^2\theta\cos\phi\sin\phi)X+(\cos\theta\sin\theta\sin\phi-\sin^2\theta\cos\phi\sin\phi)Y & 0 \end{vmatrix}$$

[35]

where

$$X = \exp[i(\hat{n}_x-1)\frac{\omega b}{c}] \qquad [36]$$

$$Y = \exp[i(\hat{n}_y-1)\frac{\omega b}{c}] \qquad [37]$$

as discussed previously. Substituting the equation for the complex refractive index (See Equation [38]) into Equations [36] and [37] results in Equations [39] and [40].

$$\hat{n} = n + i\,\frac{\alpha c}{2\omega} \qquad [38]$$

$$X = \exp[i(n_x + i\frac{\alpha_x c}{2\omega} - 1)\frac{\omega b}{c}] \qquad [39]$$

$$Y = \exp[i(n_y + i\frac{\alpha_x c}{2\omega} - 1)\frac{\omega b}{c}] \qquad [40]$$

where α_x and α_y are the Naperian absorption coefficients for the π and σ components, respectively.

Substituting the result for [A] (See Equation [35]) back into Equation [34], results in the following equation for the light transmitted through the polarizers.

$$I_T = \tfrac{1}{2}I_0\exp[-\tfrac{1}{2}(\alpha_x+\alpha_y)b]\{(\cos\theta\cos^2\phi+\sin\theta\cos\phi\sin\phi)^2\exp[\tfrac{1}{2}(\alpha_y-\alpha_x)b] +$$
$$(\cos\theta\sin^2\phi-\sin\theta\cos\phi\sin\phi)^2\exp[\tfrac{1}{2}(\alpha_x-\alpha_y)b] +$$
$$(\cos2\theta\cos^2\phi\sin^2\phi-\cos\theta\sin\theta\cos\phi\sin\phi\cos2\phi)\cdot$$
$$(\exp[i(n_x-n_y)\frac{\omega b}{c}] + \exp[i(n_y-n_x)\frac{\omega b}{c}])\} \qquad [41]$$

By using the trigonometric identity for the cos x in Equation [42] Equation [41] reduces to its final form, Equation [21].

$$\cos x = \frac{e^{ix} + e^{-ix}}{2} \qquad [42]$$

$$I_T = \tfrac{1}{2}I_0\exp[-\tfrac{1}{2}(\alpha_x+\alpha_y)b]\{(\cos\theta\cos^2\phi+\sin\theta\cos\phi\sin\phi)^2\exp[\tfrac{1}{2}(\alpha_y-\alpha_x)b] +$$
$$(\cos\theta\sin^2\phi-\sin\theta\cos\phi\sin\phi)^2\exp[\tfrac{1}{2}(\alpha_x-\alpha_y)b] +$$
$$2(\cos2\theta\cos^2\phi\sin^2\phi-\cos\theta\sin\theta\cos\phi\sin\phi\cos2\phi)\cos[(n_x-n_y)\frac{\omega b}{c}]\} \qquad [21]$$

Two limiting cases were also derived. If the axis of the first polarizer is set at a 45° angle to the magnetic field so that $\phi = 45°$ and $\cos\phi = \sin\phi$ at this angle, Equation [21] reduces to Equation [45] with the use of the trigonometric identities in Equations [43] and [44]

$$\cosh x = \frac{e^{x} + e^{-x}}{2} \qquad [43]$$

$$\sinh x = \frac{e^{x} - e^{-x}}{2} \qquad [44]$$

$$I_T = \tfrac{1}{4}I_0\exp[-\tfrac{1}{2}(\alpha_x+\alpha_y)b]\{\cosh[\tfrac{1}{2}(\alpha_x-\alpha_y)b]-\sin2\theta\sinh[\tfrac{1}{2}(\alpha_x-\alpha_y)b] +$$
$$\tfrac{1}{2}\cos2\theta\cos[\frac{\omega b}{c}(n_x-n_y)]\} \qquad [45]$$

If the squared CFS system is now considered where $\theta = 90°$ as used in the majority of this study, Equation [45 reduces to the final result shown in Equation [22].

$$I_T = \frac{1}{4}I_0 \exp[\ \tfrac{1}{2}(\alpha_x+\alpha_y)b]\{\cosh[\tfrac{1}{2}(\alpha_x-\alpha_y)b] - \cos \tfrac{\omega b}{c}(n_x-n_y)]\} \quad [22]$$

APPENDIX II
LIST OF ABBREVIATIONS

CFS -- coherent forward scattering atomic spectrometry

AAS — atomic absorption spectrometry

ZAAS -- Zeeman atomic absorption spectrometry

AFS — atomic fluorescence spectrometry

AES — atomic emission spectrometry

LOD — limit of detection

UAR -- useful analytical range

AM — amplitude modulation

CW laser — continuous wavelength laser

REFERENCES

1. Robert W. Wood, *Physical Optics*, Dover Publications Inc., New York (1967), 669.

2. A. Walsh, *Spectrochim. Acta*, *7*, 108 (1955).

3. H. Prugger, 2nd. International Conference, *Abstracts of Papers*, F-6 at Sheffield (1969).

4. H. Prugger and R. Torge, German Pat. 1964469 Claim Priority, Dec. 23rd (1969).

5. T. Hollander, B.J. Jansen, J.J. Plaat, and Th.J. Alkamade, *J. Quant. Spectrosc. Radiat. Transfer*, *10*, 1301 (1970).

6. C. Parker, Australia Pat. PA3643/11 Claim Priority, Jan. 5th (1977).

7. H. Koizumi, K. Yasuda, and M. Katayama, *Anal. Chem.*, *49*, 1106 (1977).

8. K. Yasuda, H. Koizumi, K. Ohisi, and T. Noda, *Prog. Analyt. Atom Spectrosc.*, *3*, 299 (1980).

9. M.T.C. De Loos-Vollebregt and L. De Galan, *Spectrochim. Acta*, *33B*, 495 (1978).

10. W. Hanle, *Z. Phys.*, *30*, 93 (1924).

11. A. Corney, B.P. Kibble, and G.W. Series, *Proc. R. Soc. A*, *293*, 70 (1966).

12. A.V. Durrant and B. Landheer, *J. Phys. B: Atom. Molec. Phys.*, *4*, 1200 (1971).

13. R. Stephens, *Can. J. Spectrosc.*, *24*, 11 (1979).

14. M. Yamamoto and S. Murayama, *J. Opt. Soc. Am.*, *69*, 781 (1979).

15. M. Yamamoto, S. Murayama, M. Ito, and M. Yasuda, *Spectrochim. Acta*, *35B*, 43 (1980).

16. J.J. Kankare and R. Stephens, *Spectrochim. Acta*, *35B*, 849 (1980).

17. J. Kankare and R. Stephens, *Appl. Spectrosc.*, *34*, 590 (1980).

18. R. Stephens, *Spectrochim. Acta*, *38B*, 1077 (1983).

19. J.J. Kankare and R. Stephens, *Spectrochim. Acta*, *38B*, 1301 (1983).

20. A.D. Kersey, J.B. Dawson, and D.J. Ellis, *Spectrochim. Acta*, *35B*, 865 (1980).

21. D.A. Church and T. Hadeishi, *Appl. Phys. Lett.*, *24*, 185 (1974).

22. R. Stephens, *Anal. Chim. Acta*, *98*, 291 (1978).

23. K. Hirokawa, *Anal. Chem.*, *52*, 1966 (1980).

24. K. Hirokawa and M. Namiki, *Spectrochim. Acta*, *36B*, 649 (1981).

25. V. Gurvinder, S. Jolly, and R. Stephens, *Spectrochim. Acta*, *39B*, 335 (1984).

26. M. Ito, *Anal. Chem.*, *52*, 1592 (1980).

27. H. Debus, W. Hanle, A. Scharmann, and P. Wirz, *Spectrochim. Acta*, *36B*, 1015 (1981).

28. K. Hirokawa and M. Namiki, *Spectrochim. Acta*, *37B*, 165 (1982).

29. P. Wirz, H. Debus, W. Hanle, and A. Scharmann, *Spectrochim. Acta*, *37B*, 1013 (1982).

30. S.R. Koirtyohann, paper no. 262, at FACSS XII, Philadelphia (1985).

31. Y. Uchida and S. Hattori, *Oyo Butiri*, *44*, 852 (1975).

32. V. Otruba, J. Jambor, J. Horak, and L. Sommer, *Skripta Fac. Sci. Nat. Ujep Brunensis, Chemia*, *1*, 1 (1976).

33. H. Koizumi and K. Yasuda, *Anal. Chem.*, *47*, 1679 (1975).

34. H. Koizumi and K. Yasuda, *Spectrochim. Acta*, *31B*, 237 (1976).

35. H. Koizumi and K. Yasuda, *Anal. Chem.*, *48*, 1178 (1976).

36. H. Koizumi and K. Yasuda, *Spectrochim. Acta*, *31B*, 523 (1976).

37. J.B. Dawson, E. Grassam, D.J. Ellis, and M.J. Keir, Analyst, 101, 315 (1976).

38. E. Grassam, J.B. Dawson, and D.J. Ellis, Analyst, 102, 804 (1977).

39. R. Stephens and D.E. Ryan, Talanta, 22, 555 (1975).

40. R. Stephens and D.E. Ryan, Talanta, 22, 659 (1975).

41. D.E. Veinot and R. Stephens, Talanta, 23, 849 (1976).

42. R. Stephens, Talanta, 24, 233 (1977).

43. T. Hadeishi and R.D. McLaughlin, Science, 174, 404 (1971).

44. T. Hadeishi, Appl. Phys. Lett., 21, 438 (1972).

45. T. Hadeishi, D.A. Church, R.D. McLaughlin, B.D. Zak, M. Nakamura, and B. Chang, Science, 187, 348 (1975).

46. T. Hadeishi and R.D. McLaughlin, Am. Lab., 7, 57 (1975).

47. T. Hadeishi and R.D. McLaughlin, Anal. Chem., 48, 1009 (1976).

48. C.H. Corliss and W.R. Bozman, Experimental Transition Probabilities for Spectral Lines of Seventy Elements, NBS Monograph 53, Washington, DC (1962).

49. F.J. Fernandez, W. Bohler, M.M. Beaty, and W.B. Barnett, At. Spectrosc., 2, 73 (1981).

50. H.G. Kuhn, Atomic Spectra, Academic Press, New York (1969), 55.

51. M.S. Epstein and J.D. Winefordner, Prog. Analyt. Atom. Spectrosc., 7, 67 (1984).

52. C.Th.J. Alkemade, W. Snellman, G.D. Boutilier, B.D. Pollard, J.D. Winefordner, T.L. Chester, and N. Omenetto, Spectrochim. Acta, 33B, 383 (1978).

53. G.D. Boutilier, B.D. Pollard, J.D. Winefordner, T.L. Chester, and N. Omenetto, Spectrochim. Acta, 33B, 401 (1978).

54. N.W. Bower and J.D. Ingle, Jr., Appl. Spectrosc., 35, 317 (1981).

55. N.W. Bower and J.D. Ingle, Jr., Anal. Chem., 49, 574 (1977).

56. K. Fujiwara, A.H. Ullman, J.D. Bradshaw, B.D. Pollard, and J.D. Winefordner, Spectrochim. Acta, 34B, 137 (1979).

57. B.D. Pollard, A.H. Ullman, and J.D. Winefordner, *Anal. Chem.*, *53*, 330 (1981).

58. G. Herzberg, *Molecular Spectra and Molecular Structure, I. Spectra of Diatomic Molecules*, D. Van Nostrand Company Inc., Princeton (1950), 298.

59. A.G. Gaydon and H.G. Wolfhard, *Flames: Their Structure, Radiation, and Temperature*, 3rd ed., Chapman and Hall, London (1970).

60. S.J. Weeks, H. Haraguchi, and J.D. Winefordner, *Anal. Chem.*, *50*, 360 (1978).

61. B.W. Smith, M.B. Blackburn, and J.D. Winefordner, *Can. J. Spectrosc.*, *22*, 57 (1977).

62. B. Smith, J.D. Winefordner, and N. Omenetto, *J. Appl. Phys.*, *48*, 2676 (1977).

63. D.J. Johnson and J.D. Winefordner, *Anal. Chem.*, *48*, 341 (1976).

64. P. Wittman and J.D. Winefordner, *Can. J. Spectrosc.*, *29*, 75 (1985).

65. H. Greenstein and C.W. Bates, Jr., *J. Opt. Soc. Am.*, *65*, 33 (1975).

66. C.Th.J. Alkemade, Tj. Hollander, W. Snellman, and P.J.Th. Zeegers, *Metal Vapors in Flames*, Pergamon Press, New York (1982), 140.

67. L.A. Davis and J.D. Winefordner, poster #214 at FACSS XII, Philadelphia (1985).

68. T.C. O'Haver, *Analyst*, *109*, 211 (1984).

69. J.M. Harnly, T.C. O'Haver, B. Golden, and W.R. Wolf, *Anal. Chem.*, *51*, 2007 (1979).

70. F.S. Chuang and J.D. Winefordner, *Appl. Spectrosc.*, *29*, 412 (1975).

71. D.J. Johnson, F.W. Plankey, and J.D. Winefordner, *Anal. Chem.*, *47*, 1739 (1975).

72. A.H. Ullman, B.D. Pollard, G.D. Boutilier, P. Hanley, and J.D. Winefordner, *Anal. Chem.*, *51*, 2382 (1979).

73. L.A. Davis, R.J. Krupa, and J.D. Winefordner, Anal. Chim. Acta, 173, 51 (1985).

74. R.J. Klueppel and J.P. Walters, Spectrochim. Acta, 35B, 431 (1980).

75. P.E. Walters, J. Lanauze, and J.D. Winefordner, Spectrochim. Acta, 39B, 125 (1984).

76. P.E. Walters, G.L. Long, and J.D. Winefordner, Spectrochim. Acta, 39B, 69 (1984).

BIOGRAPHICAL SKETCH

Lori Ann Davis was born in DeLand, Florida, on December 2, 1960. She attended DeLand Senior High School graduating in 1978. She then attended Emory University in Atlanta, Georgia, and graduated with her B.S. in chemistry in June of 1982. From that time she attended the University of Florida, earning her M.S. in chemistry in August of 1984. Her studies at the University of Florida continued under the direction of Dr. James D. Winefordner until her graduation in August of 1986 with her Ph.D. in chemistry.

I certify that I have read this study and that in my opinion it conforms to acceptable standards of scholarly presentation and is fully adequate, in scope and quality, as a dissertation for the degree of Doctor of Philosophy.

James D Winefordner

James D. Winefordner, Chairman
Graduate Research Professor of Chemistry

I certify that I have read this study and that in my opinion it conforms to acceptable standards of scholarly presentation and is fully adequate, in scope and quality, as a dissertation for the degree of Doctor of Philosophy.

J. G. Dorsey

John G. Dorsey
Associate Professor of Chemistry

I certify that I have read this study and that in my opinion it conforms to acceptable standards of scholarly presentation and is fully adequate, in scope and quality, as a dissertation for the degree of Doctor of Philosophy.

Alex E. Green

Alex E. Green
Graduate Research Professor of
Mechanical Engineering

This dissertation was submitted to the Graduate Faculty of the Department of Chemistry in the College of Liberal Arts and Sciences and to the Graduate School and was accepted as partial fulfillment of the requirements for the degree of Doctor of Philosophy.

August, 1986

Dean, Graduate School